



ELSEVIER

Contents lists available at SciVerse ScienceDirect

Earth and Planetary Science Letters

journal homepage: www.elsevier.com/locate/epsl

The deep structure of the North Anatolian Fault Zone



Andreas Fichtner^{a,(*)}, Erdinc Saygin^b, Tuncay Taymaz^c, Paul Cupillard^d, Yann Capdeville^e,
Jeannot Trampert^f

^a Department of Earth Sciences, Department of Earth Sciences, ETH Zurich, Switzerland

^b Research School of Earth Sciences, The Australian National University, Canberra, Australia

^c Department of Geophysical Engineering, Istanbul Technical University, Istanbul, Turkey

^d Nancy School of Geology, Computer Science Department, Nancy, France

^e Laboratoire de Planétologie et de Géodynamique de Nantes, Nantes, France

^f Department of Earth Sciences, Utrecht University, Utrecht, The Netherlands

ARTICLE INFO

Article history:

Received 7 January 2013

Received in revised form

18 April 2013

Accepted 19 April 2013

Editor: P. Shearer

Available online 17 May 2013

Keywords:

North Anatolian Fault Zone
tomography

full-waveform inversion

continental strike-slip faults

ABSTRACT

Multi-scale full waveform inversion of complete continental- and regional-scale seismograms reveals the crustal and upper-mantle signature of the North Anatolian Fault Zone which shapes the neotectonics of Turkey and the eastern Mediterranean. Within the crust, the fault zone is mostly bounded by several high-velocity blocks, suggesting that it developed along the edges of continental fragments with high rigidity. Below the crust, the surface expression of the eastern and central parts of the North Anatolian Fault Zone correlate with a pronounced low-velocity band that extends laterally over 600 km. Around 100 km depth, the low-velocity band merges into the shallow Anatolian asthenosphere, thereby providing a link to the Kurka–Afyon–Isparta Volcanic Field and the Central Anatolian Volcanics. We interpret the low-velocity band beneath the North Anatolian Fault Zone as the upper-mantle expression of the Tethyan sutures that formed 60–15 Ma ago as a result of Africa–Eurasian convergence. The structurally weak suture facilitated the formation of the younger (less than 10 Ma) crustal fault zone. In this sense, the North Anatolian Fault Zone is not only a crustal feature, but a narrow zone of weakness that extends into the upper mantle.

© 2013 Elsevier B.V. All rights reserved.

1. Introduction

The North Anatolian Fault Zone (NAFZ, see Fig. 1) is one of the Earth's major continental strike-slip fault zones that shapes the neotectonic evolution of Turkey and the eastern Mediterranean region. It is characterised by strong seismic activity, posing a high risk to densely populated areas. Despite its importance for the general understanding of large strike-slip fault systems, Eurasian tectonics and earthquake cycle modelling, the deep structure of the NAFZ remains largely enigmatic. Key to further progress are detailed tomographic models of the Anatolian region that provide a consistent 3D picture of both the crust and the upper mantle.

The NAFZ, with its most prominent member the North Anatolian Fault (NAF), extends for ~1500 km from the Karliova triple junction in eastern Anatolia to the Sea of Marmara. It began to develop in the form of a broad shear zone 11–5 Ma ago in response to the north–south convergence of the Eurasian and Arabian plates, and the resulting south–west extrusion of the Anatolian block (Barka, 1992). Starting ~11 Ma ago in the eastern part of the shear zone, strain localisation propagated westward, thereby forming a narrow fault zone that reached the Sea of Marmara no

earlier than 200 ka ago (Şengör et al., 2005). Today, the width of the fault zone increases from ~10 km in the east to ~100 km in the west (Şengör et al., 2005).

Along much of its length, the NAFZ is located in the vicinity of the Intra-Pontide and İzmir–Ankara–Erzincan sutures (Fig. 1). Both sutures formed during the closure of the Neotethyan Ocean 60–15 Ma ago as a result of Africa–Eurasian convergence (Okay and Tüysüz, 1999; Bozkurt, 2001). This suggests a close relation between the near-surface expression of the NAFZ and deeper lithospheric zones of weakness that remains to be explored.

A remarkably regular migration of major earthquakes along the NAF from east to west over a time scale of several decades was recognised as early as 1944 (Egeran and Lahn, 1944), and later modelled successfully by stress propagation (Stein et al., 1997). Shear zone evolution and earthquake migration can be simulated with increasing accuracy when detailed information on the lithospheric structure is available (Lyakhovskiy and Ben-Zion, 2009; Takeuchi and Fialko, 2012), which underlines the need for highly resolved tomographic models of the crust and uppermost mantle.

Owing to its elevated seismic risk and importance for Eurasian neotectonics, Anatolia has been the subject of various recent tomographic studies. While crustal structure was imaged with local earthquake tomography (Koulakov et al., 2010; Yolsal-Çevikbilen et al., 2012), receiver functions (Saunders et al., 1998; Vanacore et al., 2013) and refraction profiles (Karabulut et al., 2003), models of the upper

(* Corresponding author. Tel.: +41 44 632 2597.

E-mail address: andreas.fichtner@erdw.ethz.ch (A. Fichtner).



Fig. 1. Neotectonic map of Anatolia, including major fault zones (black lines, after Bozkurt, 2001), sutures of the Tethyan ocean (blue lines, after Okay and Tüysüz, 1999) and Holocene volcanoes (red diamonds, after Siebert and Simkin, 2002). The North Anatolian Fault Zone (NAFZ) is marked by dashed transparent lines (adapted from Şengör et al., 2005). (For interpretation of the references to colour in this figure legend, the reader is referred to the web version of this article.)

mantle were obtained from teleseismic body and surface waves (Biryol et al., 2011; Bakırcı et al., 2012; Salaün et al., 2012). Inversions for either the crust or the mantle require assumptions on one of them, which can lead to artifacts in the tomographic model, especially at shallow depth (Bozdağ and Trampert, 2008; Ferreira et al., 2010). A consistent model of both crust and upper mantle beneath Anatolia is still not available, due to the difficulty of simulating and inverting broadband seismic wavefields in Earth models with strong 3D heterogeneities.

To overcome this difficulty, we developed a multi-scale full waveform inversion that integrates teleseismic and regional data. This allows us to simultaneously constrain the crust and the upper mantle, thereby shedding light onto the interaction between deep lithospheric structure and shallow tectonic features.

2. Data and tomographic technique

The key element of our tomographic technique is a spectral-element method (SEM) for the solution of the seismic wave equation, described in Fichtner et al. (2009). The SEM produces highly accurate synthetic seismograms for Earth models with strong 3D heterogeneities, and in particular for laterally variable crustal structure (Komatitsch and Vilotte, 1998; Komatitsch and Tromp, 2002). In contrast to classical body or surface wave tomography, full waveform inversion exploits information from complete seismograms, including body and surface waves, for the benefit of improved tomographic resolution (e.g. Chen et al., 2007; Tape et al., 2010; Fichtner et al., 2010; Zhu et al., 2012; Rickers et al., in preparation). The major innovation of this study is the simultaneous inversion of regional and teleseismic data within the framework of full waveform inversion. This allows us to constrain both crustal and upper-mantle structure beneath Anatolia, and to avoid contamination of the Anatolian model by unknown Earth structure outside that region.

2.1. Data selection and processing

We obtained three-component seismic data from the data centres of IRIS, ORFEUS, the Kandilli Observatory and Earthquake Research Institute (UDIM), the National Seismic Array of Turkey (AFAD-DAD) and the IberArray project. From the available data we selected recordings where the noise estimated from waveforms prior to the arrival of the first P wave is negligible compared to the differences between observed and synthetic seismograms. Our final data set

contains 16,836 seismograms from 113 earthquakes that occurred in Europe and western Asia between 2005 and 2011. The data were recorded on nearly 800 stations. The magnitude of the earthquakes ranges between 4.9 and 6.8, so that finite-source effects can be ignored when recordings close to the source are rejected. A summary of the source–receiver distribution is provided in Fig. 2.

Of the 16,836 seismograms in the complete data set, 2312 originate from 29 earthquakes in the Anatolian region that were recorded within Anatolia itself. We analyse these regional data in the period range from 8 to 50 s. Short periods below ~ 30 s allow us to resolve crustal structure beneath Anatolia. The remaining 14,524 seismograms originate from 84 earthquakes throughout Europe and western Asia. These continent-wide data are analysed in the period range from 30 to 200 s. They are mostly sensitive to upper-mantle structure but also to the broad patterns of crustal heterogeneities.

2.2. Iterative non-linear inversion

The goal of our tomographic inversion is to find a 3D Earth model that minimises the cumulative misfit between observed and synthetic seismograms of all source–receiver pairs. For this, we start with SEM simulations of the earthquakes in our data set using a 3D initial model of the crust (Meier et al., 2007) and mantle (Ritsema et al., 1999), as well as initial earthquake source parameters obtained from the Centroid Moment Tensor Catalogue (www.globalcmt.org). The synthetic seismograms from these initial simulations are then compared to the observed seismograms, using time–frequency phase misfits (Fichtner et al., 2008). Time–frequency phase misfits have various advantageous properties that are crucial for the success of a regional-to global-scale full waveform inversion. They are not affected by the absolute amplitudes of the seismogram, and they automatically balance small- and large-amplitude waveforms. Furthermore, the time–frequency phase measurements can be applied to complete seismograms, without the need to identify or window particular seismic phases. To improve the quality of the tomographic model, we merely apply windows to eliminate time intervals where observed and synthetic waveforms are more than a half cycle out of phase.

To successively update the initial model, we compute sensitivity kernels of the cumulative phase misfit with the help of adjoint techniques (e.g. Tarantola, 1988; Tromp et al., 2005; Fichtner et al., 2006; Liu and Tromp, 2008; Chen, 2011). The sensitivity kernels determine the descent direction in an iterative non-linear conjugate-gradient minimisation. We simultaneously update the P wave velocity, v_P , the velocity of horizontally polarised S waves, v_{SH} , and the velocity

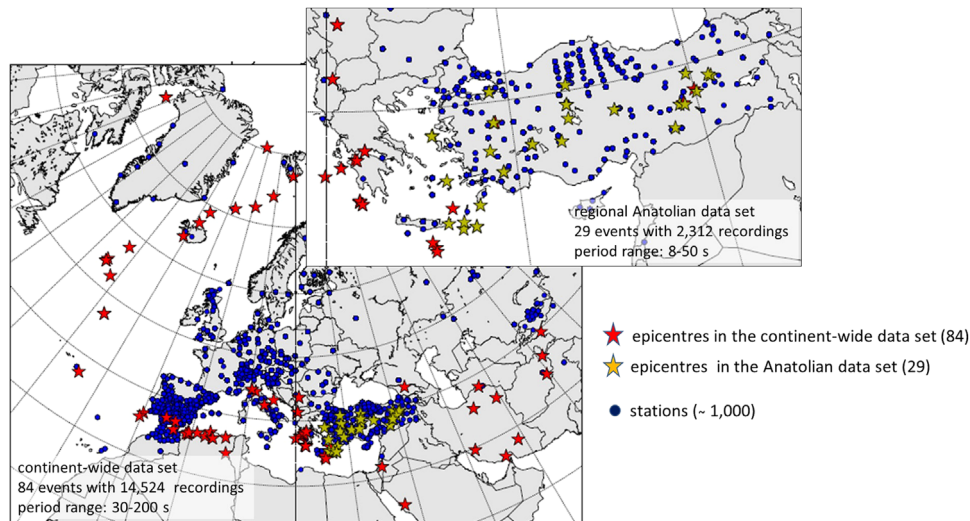


Fig. 2. Summary of data used in the tomographic inversion. Shown is the distribution of receivers (blue dots), epicentres in the continent-wide data set (red stars) and epicentres in the regional Anatolian data set (yellow stars). Also indicated are the period ranges and the volumes of the continent-wide and regional data subsets, respectively. (For interpretation of the references to colour in this figure legend, the reader is referred to the web version of this article.)

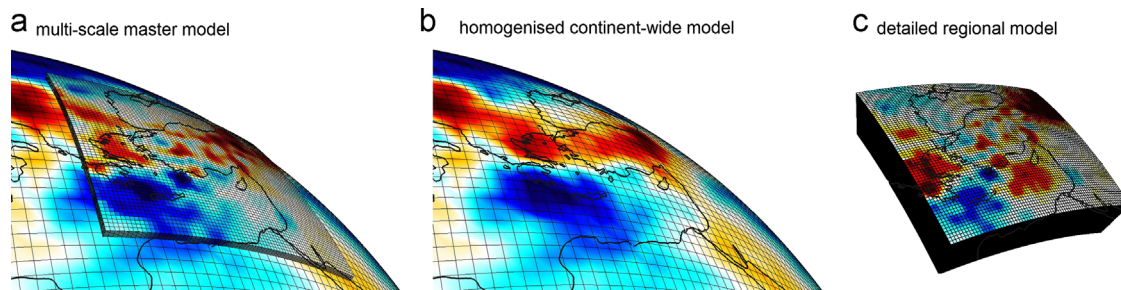


Fig. 3. Illustration of the multi-scale approach and the domain decomposition: (a) The master model has a variable grid size. A fine grid is used for the Anatolian region where short-period (8–50 s) waves are propagated. A coarser grid is used throughout the remaining study region. Superimposed on the figure of the model are the elements used in the spectral-element simulations. (b) The coarsely gridded version of the master model is obtained by upscaling the detailed structure on the finely gridded Anatolian subvolume using the 3D variant of non-periodic homogenisation (Capdeville et al., 2010a, 2010b). The upscaling procedure introduces apparent anisotropy that the wavefield simulations must account for. The coarsely gridded model is used for the simulation of the longer-period (30–200 s) data across the whole continent. (c) The small Anatolian subvolume is extracted from the master model in order to simulate shorter-period regional data that are capable of resolving crustal structure.

of vertically polarised S waves, v_{SV} . Furthermore, we re-invert for the earthquake source parameters every three iterations.

During the iterative inversion we successively broaden the period range to avoid trapping in a local minimum. In the first iterations on the continental scale, we use seismograms with periods from 120 to 200 s. The period band is extended to 30–200 s during the last few iterations. On the regional scale, we start with a narrow band from 30 to 50 s, broadened to 8–50 s in the last iterations. The iterative improvement of the model allows us to increase the number of recordings that can be incorporated into the inversion because observed and synthetic waveforms become sufficiently similar to make a meaningful phase measurement. The algorithm successively explains waveforms that were not previously used in the inversion, thereby providing additional evidence for convergence towards the global optimum.

2.3. Multi-scale full waveform inversion

The key methodological development of this study consists in the simultaneous full waveform inversion of seismic data sets on different spatial scales, i.e. on a continental scale (Europe and western Asia) and a regional scale (Anatolia). This development is essential for the resolution of both crustal and upper-mantle structure, needed to draw inferences on the interaction between the brittle and ductile parts of the lithosphere.

Upper-mantle structure can be resolved using continental-scale data with epicentral distances above 5° and comparatively long periods between 30 and 200 s. For these periods, the grid point spacing in the SEM mesh is required to be ~ 9 km, meaning that simulations for the whole continent are computationally feasible. To resolve crustal structure beneath Anatolia, regional seismic waveforms with periods below 10 s should ideally be used. The required grid point spacing is then ~ 3 km. Thus, the grid used for the continental-scale wavefield simulations must at least be refined within the Anatolian region. Despite being local, this refinement of the grid by a factor of 3, forces a reduction of the time step by a factor of 3 as well, meaning that the time required by a simulation is three times as long as without the grid refinement. Further refinements of the grid, e.g. to incorporate high-frequency local data in an area of special interest, would rapidly increase the computational requirements beyond an acceptable level.

To make a simultaneous inversion for crust and mantle practically feasible, we developed an efficient multi-scale full waveform inversion based on a decomposition of the computational domain and the solution of multiple wave propagation problems. Our method rests on the definition of a master model with a refined grid in the Anatolian region and a coarser grid beneath the rest of the continent (Fig. 3a). In the first iteration, we upscale the finely-gridded Anatolian submodel onto a coarser grid that can be used for the continent-wide longer-period simulations (Fig. 3b). This upscaling is based on the 3D variant of non-periodic homogenisation (Capdeville et al., 2010a, 2010b), and

it introduces apparent anisotropy that must be accounted for in the numerical simulations. On the coarser grid, we perform one iteration with the continental-scale data, and the resulting update is added to the master model. From the updated master model, we extract the finely-gridded Anatolian submodel (Fig. 3c). The SEM simulation of the shorter-period regional data is then restricted to a small model subvolume that comprises the crust and upper mantle beneath Anatolia. Since the Anatolian subvolume is small, the numerical simulations are sufficiently inexpensive, despite the fine grid spacing. Based on the regional simulations, we compute an update for Earth structure beneath Anatolia that we add to the master model. We then iterate this alternating procedure. For further details on the multi-scale approach, the reader is referred to Fichtner et al. (in press).

We stopped the inversion after 42 iterations, when most synthetics explained the data to within the noise. Before presenting the final model, ECOS.TU.42, we provide an analysis of its spatial resolution.

2.4. Resolution analysis

A detailed resolution analysis for the isotropic S velocity, $v_S = 2v_{SH}/3 + v_{SV}/3$, is presented in Fig. 4. Shown are the resolution lengths in the E–W and N–S directions, respectively, as a function of position in the 3D model volume. The resolution length is defined as the width of the point-spread function, measured along a specified direction, i.e. E–W or N–S in this case. Resolution lengths and other proxies for tomographic resolution can be computed efficiently with the help of SEM and second-order adjoints, so that finite-frequency and 3D wave propagation effects are accurately accounted for (Fichtner and Trampert, 2011a, 2011b). The presented resolution analysis is more complete and diagnostic than checkerboard-type synthetic inversions that are highly dependent on the characteristics of the input structure and provide potentially misleading results (Lévêque et al., 1993).

At 20 km depth the resolution length in both E–W and N–S directions is ~ 25 km throughout most of Anatolia (Fig. 4a). This means that structural features that are more than 25 km wide are resolved, and can thus be interpreted. From 50 km to 100 km

depth, resolution lengths beneath Anatolia are generally below 50 km. Outside Anatolia, where structure is constrained only by the longer-period data set, resolution length increases beyond 80 km. In general, the minimum resolution length tends to increase slightly with increasing depth.

To visualise the larger resolution length outside Anatolia, a resolution analysis for the complete model is shown in Fig. 4b at 50 km depth and with a wider colour scale. Independent of depth, resolution is best beneath southern Europe and the eastern Mediterranean where most of the earthquakes and stations cluster. At 50 km depth, resolution lengths vary between 100 km and 200 km throughout most of Europe.

As demonstrated in Fichtner et al. (in press), the Anatolian part of ECOS.TU.42 reproduces Moho depth estimates from receiver function studies (Vanacore et al., 2013), indicating that vertical resolution within the lithosphere is comparable to that of receiver function inversions.

ECOS.TU.42 is the first model that jointly resolves crustal and mantle structure, thereby going beyond the classic separation of crustal studies via local tomography, receiver functions and refraction profiles (Koulakov et al., 2010; Yolsal-Çevikbilen et al., 2012; Saunders et al., 1998; Vanacore et al., 2013; Karabulut et al., 2003), and mantle tomography based on teleseismic body and surface waves (Biryol et al., 2011; Bakırcı et al., 2012; Salaün et al., 2012). Good resolution of the boundary region between crust and mantle is essential to understand interactions between mantle convection and near-surface tectonics.

3. Shear velocity distribution of model ECOS.TU.42 beneath Europe and western Asia with focus on the Anatolian region

Horizontal slices through the complete continent-wide distribution of the isotropic S velocity, obtained after 42 iterations, are shown in Fig. 5. The model confirms well-established features, including the anomalously high velocities of the East European Platform, the low-velocity Iceland plume, and the high velocities of the Hellenic Slab.

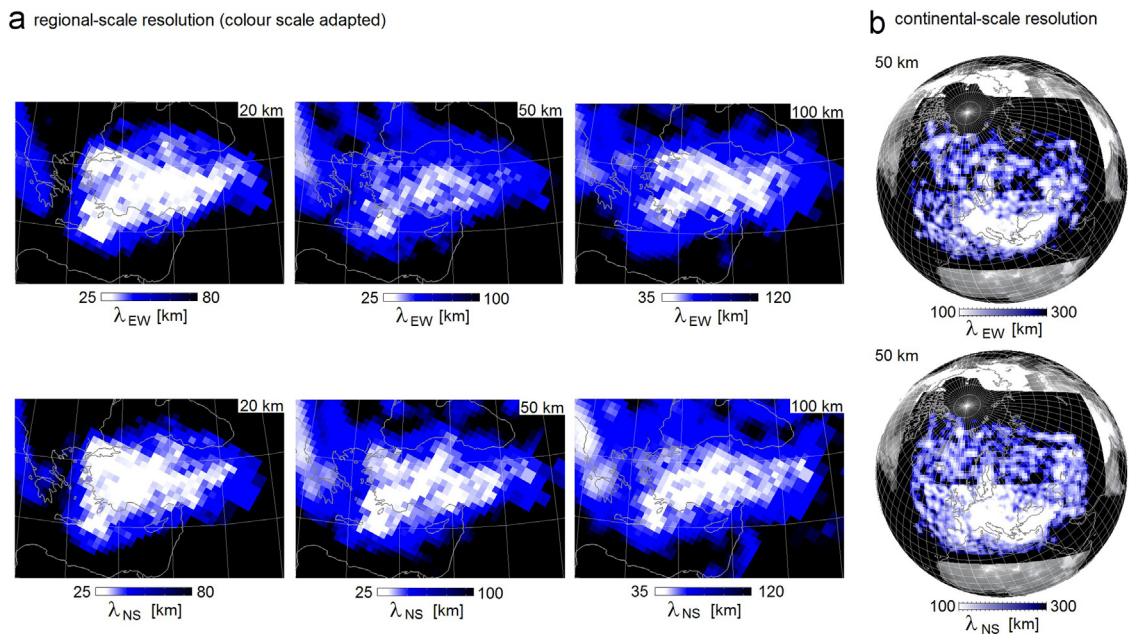


Fig. 4. Resolution analysis for the isotropic S velocity, v_S . Shown is the resolution length for model ECOS.TU.42 in the E–W direction (λ_{EW} , top row) and in the N–S direction (λ_{NS} , bottom row) as a function of position in the 3D model volume. The resolution length is defined as the width of the point spread function measured along a specified direction; either E–W or N–S in this case: (a) Distribution of resolution lengths in the Anatolian region. (b) Resolution lengths in the whole model, shown with an adapted colour scale. (For interpretation of the references to colour in this figure legend, the reader is referred to the web version of this article.)

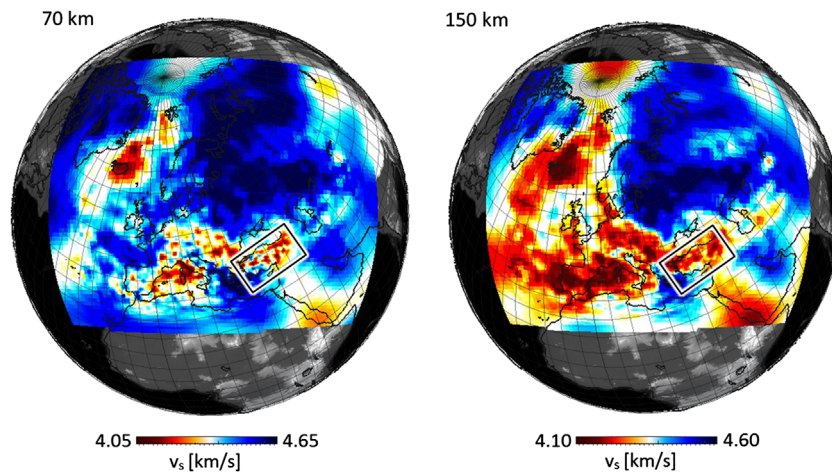


Fig. 5. Horizontal slices through the isotropic S velocity, v_s , at 70 km and 150 km depth beneath Europe and western Asia. The Anatolian region where shorter-period data have been incorporated is marked by the black rectangle. Details of the Anatolian region are shown in Figs. 6–8.

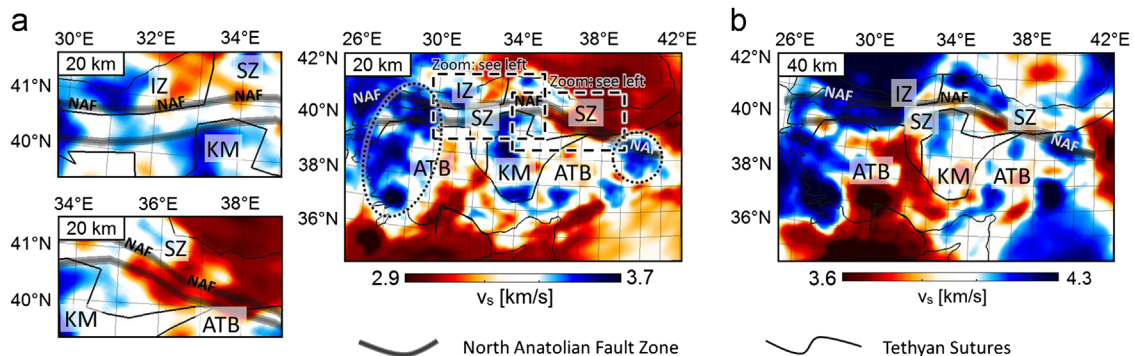


Fig. 6. Horizontal slices through the isotropic S velocity, v_s , at 20 km (a) and 40 km (b) depth. Indicated are the surface expressions of the NAFZ and Tethyan sutures. The North Anatolian Fault (NAF) marks the northern boundary of the NAFZ. Dashed rectangles mark regions that are amplified in the two leftmost panels of the figure. Dotted ellipses indicate thin (20–30 km) crust as inferred from receiver function analysis (Vanacore et al., 2013). Key to marked features: ATB, Anatolide–Tauride Block; IZ, Istanbul Zone; KM, Kırşehir Massif; SZ, Sakarya Zone.

In the following paragraphs, we focus our analysis on the Anatolian region where the incorporation of shorter-period regional data provides a particularly high resolution. This allows us to study the imprint of the NAFZ on both crustal and upper-mantle structure.

3.1. The signature of the NAFZ in the crust and crust–mantle transition

The crustal structure of Anatolia is complicated by the successive amalgamation of continental fragments during the closure of the Tethys ocean (Okay and Tüysüz, 1999). The resulting seismic velocity structure is a combination of compositional effects from widely varying rock types, thermal effects related to recent volcanism, and variations in Moho depth that can be difficult to distinguish from volumetric velocity variations. Despite these complexities, a crustal signature of the NAFZ can be distinguished throughout most of its length.

From 35°E to 38°E the position of the NAFZ correlates with a low-velocity streak visible in the 20 km slice of Fig. 6a. This feature could be the deep expression of several fault-related basins (e.g. Barka, 1992; Şengör et al., 2005). However, the extension of the low-velocity streak to greater depth and into the lithospheric mantle favours a relation to the bulk properties of the persistently weak Tethys suture (see Fig. 7 and Section 3.2).

A high-velocity block bounds the NAFZ to the south near 33°E. The block boundaries, however, do not coincide with the surface trace of the İzmir–Ankara–Erzincan suture which separates the Sakarya Zone from the Kırşehir massif (see Fig. 1). This suggests that the surface-geologic evidence for the western boundary of the Kırşehir massif may not be representative of its deeper crustal structure. A second high-velocity block bounds the NAFZ to the north, around 31°E. It corresponds to the western part of the İstanbul zone, which is characterised by crystalline Precambrian basement.

Strongly elevated S velocities of ~3.7 km/s appear at 20 km depth beneath the eastern- and westernmost segments of the NAFZ. Instead of being volumetric velocity perturbations related to thermal or compositional anomalies, these high velocities represent lower-crustal or upper-mantle material in regions where receiver function studies (Saunders et al., 1998; Vanacore et al., 2013) attest to the presence of a shallow (20–30 km) Moho. This effect is particularly pronounced in western Anatolia where crustal extension in response to slab roll-back in the Aegean exposes lower-crustal material at the surface (e.g. van Hinsbergen et al., 2010).

Some of the large-scale characteristics observed so far continue into the crust–mantle transition near 40 km depth (Fig. 6b). These include various high-velocity blocks bounding the NAFZ to the south and the north. The neutral to slightly lowered velocities at 20 km depth beneath the central part of the NAFZ develop into a more pronounced low-velocity band. This trend continues into the lithospheric mantle, as we will discuss in the following paragraphs.

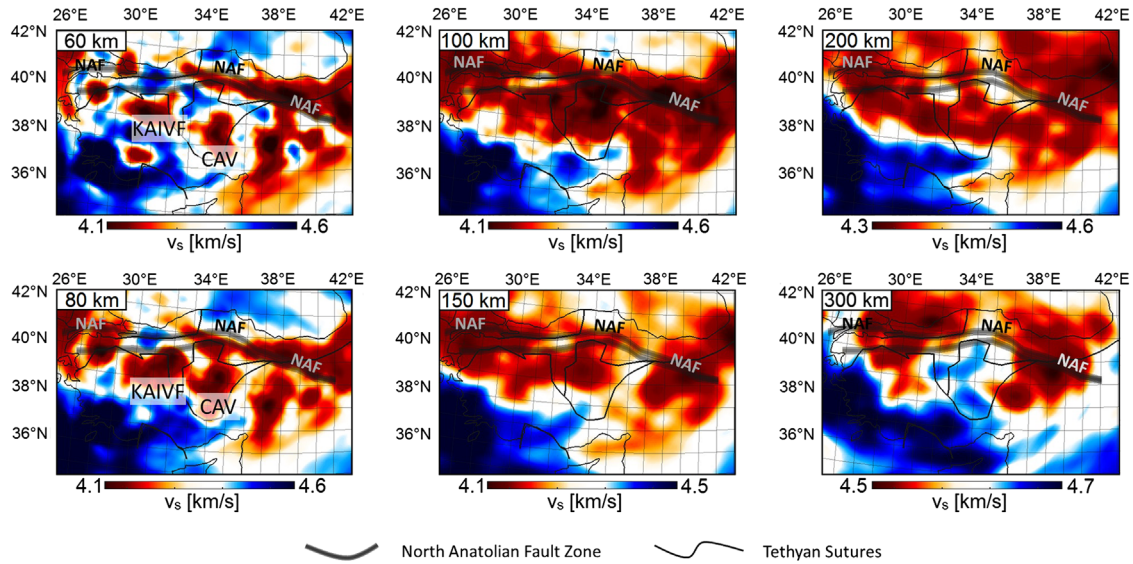


Fig. 7. Horizontal slices through the isotropic S velocity, v_s , from 60 km to 300 km depth. Indicated are the surface expressions of the NAFZ and Tethyan sutures. Key to marked features: CAV, Central Anatolian Volcanics; KAIVF, Kirka-Afyon-Isparta Volcanic Field; NAF, North Anatolian Fault.

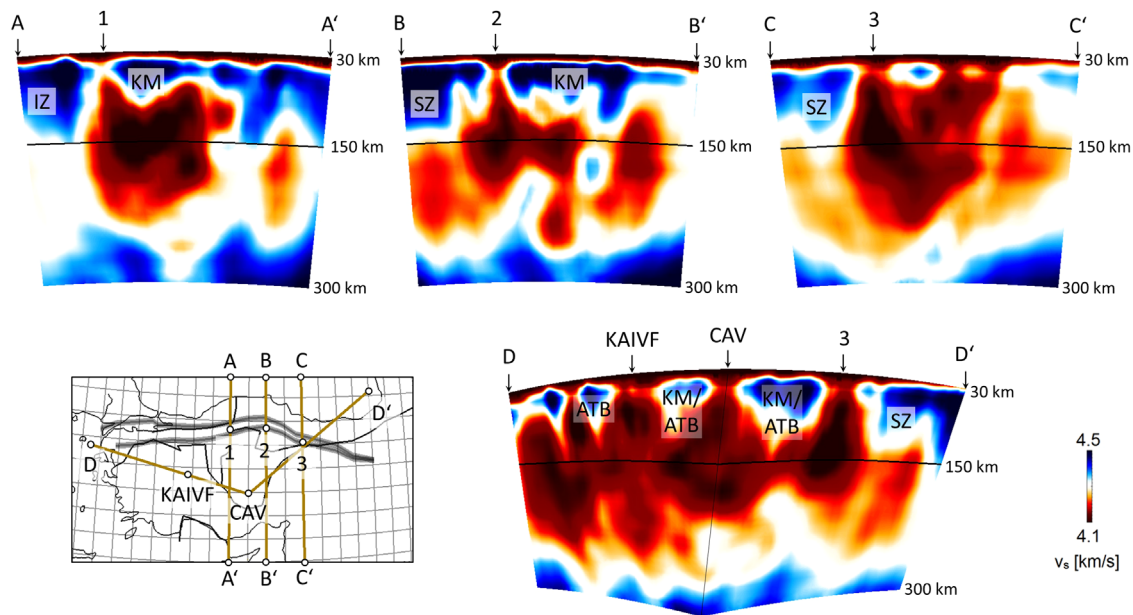


Fig. 8. Vertical slices through the isotropic S velocity, v_s , of ECOS.TU.42, stretched vertically by a factor of 3. Key to marked features: ATB, Anatolide-Tauride Block; CAV, Central Anatolian Volcanics; IZ, Istanbul Zone; KAIVF, Kirka-Afyon-Isparta Volcanic Field; KM, Kırşehir Massif; SZ, Sakarya Zone.

3.2. The upper-mantle expression of the NAFZ

The signature of the NAFZ is most visible from 50 to 80 km depth (Fig. 7) where the complexities of crustal structure are absent. There it appears as a low-velocity band extending for nearly 600 km from 32°E to 40°E. Around 60 km depth, the band is 50–100 km wide, and therefore well resolved, as indicated by the resolution analysis shown in Fig. 4. Except for the easternmost part of the NAFZ (37°E–40°E) the lithospheric low-velocity band does not follow precisely the main strand of the North Anatolian Fault (NAF) which is the most prominent member of the NAFZ. Instead, it diverges southward in the direction of the Ezinepazar-Sungurlu Fault Zone (Fig. 1), before bending northward to again meet the NAF near 32°E.

The vertical slices in Fig. 8 reveal relations between the lithospheric expression of the NAFZ and neighbouring structural features. From ~50 km depth, the low-velocity band (points 1–3 in Fig. 8) continues vertically to > 100 km depth, where it gradually merges into a broad region with S velocities below 4.2 km/s, that we associate with the shallow Anatolian asthenosphere (sections AA', BB' and CC' in Fig. 8). Between 100 and 200 km depth, the asthenosphere also provides a connection between the low-velocity band of the NAFZ (point 3 in section DD' of Fig. 8) and the anomalously low velocities of the Central Anatolian Volcanics (CAV) and the Kirka-Afyon-Isparta Volcanic Field (KAIVF). To depths of ~100 km, low velocities associated with the NAFZ are bounded by the high-velocity lithosphere of the Istanbul and Sakarya Zones to the north, and the Kırşehir Massif and the Anatolide-Tauride Block to the south.

4. Discussion

4.1. Origin of the fault zone signature

Within the crust, the NAFZ is mostly characterised by neutral to lower than average velocities that are bounded by high-velocity blocks. This indicates that the crustal fault zone preferentially developed along the edges of high-rigidity blocks. In regions where the crust is unusually thin (< 20–30 km), a clear signature of the NAFZ cannot be found. This is the case, for instance, in western Anatolia where the seismic velocity structure is dominated by the recent extensional tectonics related to slab roll-back in the Aegean. While the resolution of both crustal and upper-mantle structure for the complete Anatolian region is unprecedented, we note that it is still not sufficient to directly image the damage zone which is only 100 m to 1 km wide in the near surface (e.g. Ben-Zion, 2008). Imaging the narrow damage zone requires the use of dedicated arrays in the vicinity of a fault (e.g. Aki and Lee, 1976; Bleibinhaus et al., 2007) and the incorporation of fault zone waves (e.g. McGuire and Ben-Zion, 2005; Lewis et al., 2007; Allam and Ben-Zion, 2012) which, however, have no resolution below a few kilometres depth.

The origin of the subcrustal fault zone expression is likely to be of combined compositional, textural and thermal origin. Along much of its length, the NAFZ follows the Intra-Pontide and İzmir–Ankara–Erzincan sutures (see Fig. 1) that delineate the boundaries of various continental fragments that collided when the Neo-Tethys ocean closed around 60 Ma ago. Sutures often persist as zones of weakness with lowered elastic moduli that manifest themselves in the form of reduced seismic velocities. The low-velocity band in Figs. 6–8 is therefore likely to represent the weak boundary between the Pontides and the Anatolides that may accommodate shear motion below the crust. In this sense, the low velocity band associated with the NAFZ is probably not a damage zone produced by the fault, but a pre-existing zone of weakness that facilitated the development a large continuous fault zone.

Near the surface, the thermal contribution to the fault zone signature seems weak, as heat flow anomalies that are obviously associated with the NAFZ are not observed (Öztürk et al., 2006). However, the connection of the low-velocity band to the asthenosphere (Fig. 8) indicates the presence of elevated temperature and partial melt at greater depth. This is supported by geochemical analyses that attest to the involvement of asthenospheric melts to volcanics erupted along the NAF 10–0.1 Ma ago. The NAFZ may have served as a channel for smaller quantities of asthenospheric material (Adiyaman et al., 2001). It follows that the low-velocity band beneath the NAFZ could partly result from upwelling asthenosphere, with lowered velocities being the consequence of elevated temperatures and melt formation in response to decompression. The thermal contribution to the fault zone signature is likely to increase with depth. However, a clear discrimination of thermal, textural and compositional effects requires a tomographic resolution that can currently not be achieved.

The absence of a clear subcrustal fault zone signature west of ~32°E can be explained by the absence of a well-localised suture at depth and insufficient strain localisation observed at the surface along the young western segments of the NAFZ. Starting around 11 Ma ago in eastern Anatolia, strain localisation propagated westward, thereby forming a narrow fault zone that reached the Sea of Marmara no earlier than 200 ka ago (Şengör et al., 2005). Therefore, the fault and suture zone beneath western Anatolia may still be too diffuse to be tomographically visible as a pronounced low-velocity band.

4.2. Improving models of fault zone evolution and stress propagation

Tomographic images produced by multi-scale full waveform inversion have the potential to improve models of both short- and

long-term lithospheric deformation related to large strike–slip faults.

On a decadal time scale, variable lithospheric structure should be incorporated into Coulomb stress models in order to improve estimates of seismic hazard and aftershock occurrence. Coulomb stress changes strongly depend on 3D structure in at least two different ways. First, the presence of heterogeneities in the crust modifies the static stress field, thereby affecting earthquake probabilities and predictions of aftershock patterns (e.g. Zhao et al., 2004; Currenti et al., 2008; Tone et al., 2009; Huang and Johnson, 2012). Second, the nature of lithospheric shear zones determines how steady slip and post-seismic relaxation transfer stress to the seismogenic portion of the fault (Stein et al., 1997). These issues are particularly relevant for the NAF where Coulomb stress models in a simple layered Earth with vertically extending faults have been used to infer an increased likelihood for large earthquakes near the northern coast of the Sea of Marmara (Parsons et al., 2000; King et al., 2001).

On time scales of several hundreds to thousands of years, models for the evolution of continental strike–slip faults are becoming increasingly realistic as our knowledge of fault zone rheology improves. These models typically assume a homogeneous substrate below the brittle crust, and then predict a shear zone in the deeper lithosphere precisely beneath the surface fault trace (e.g. Lyakhovskiy and Ben-Zion, 2009; Takeuchi and Fialko, 2012). Our tomographic model indicates that real fault zones are more complicated. Their nature is strongly affected by ancient tectonic features, such as rigid blocks and persistently weak suture zones, that were already in place prior to the formation of the fault zone itself. These geologic complexities should be taken into account to further improve the modelling of subcrustal shear zones beneath continental strike–slip faults.

5. Conclusions

We developed a multi-scale full seismic waveform inversion that simultaneously inverts complete continental- and regional-scale seismograms for both crustal and upper-mantle structure. The application of multi-scale full waveform inversion to the Anatolian region reveals the deep structure of the NAFZ and its relation to Tethyan sutures.

Within the crust, the NAFZ is mostly bounded by high-velocity blocks, suggesting that the fault zone developed along the edges of high-rigidity blocks. Exceptions are regions with anomalously thin crust, e.g. in easternmost and western Anatolia, where a clear fault zone signature is not present.

The surface expression of the NAFZ correlates with an upper-mantle low-velocity band that extends laterally for 600 km from 32°E to 40°E. Near 100 km depth, the low-velocity band merges into the shallow Anatolian asthenosphere, which also provides a connection to volcanic provinces observed at the surface. We interpret the low velocities as the deep expression of the persistently weak Tethys suture that facilitated the development of the large-scale crustal fault zone. Geochemical analysis also suggests partial melt and elevated temperatures may contribute to reduced seismic velocities.

Our results indicate that the NAFZ is not only a crustal feature. It has a clear expression within the lithospheric mantle, suggesting that the evolution of the young (≤ 10 Ma) crustal fault zone is controlled by older (60–15 Ma) and structurally weak suture zones at greater depth. Multi-scale models like the one presented here have the potential to improve simulations of stress-propagation and long-term fault zone evolution.

Acknowledgements

Andreas Fichtner was funded by The Netherlands Research Center for Integrated Solid Earth Sciences under project number ISES-MD.5. Tuncay Taymaz thanks the Alexander von Humboldt-Stiftung, TÜBİTAK, TÜBA and İTÜ for partial financial support. Erdinc Saygin was supported through Australian Research Council Grants. The contributions of Yann Capdeville and Paul Cupillard were supported by the ANR mémé (ANR-10-Blanc-613) project. Numerous computations were done on the Huygens IBM p6 supercomputer at SARA Amsterdam. Use of Huygens was sponsored by the National Computing Facilities Foundation (N.C.F.) under the project SH-161-09 with financial support from the Netherlands Organisation for Scientific Research (N.W.O.). We would like to thank AFAD-DAD and BU-Kandıllı Observatory-UDİM for providing earthquake data-set on Turkish stations. Antonio Villaseñor is gratefully acknowledged for providing IberArray data. This work would not have been possible without the support of Yesim Çubuk, Seda Yolsal-Çevikbilen, Theo van Zessen, Brian Kennett, Moritz Bernauer, Giampiero Iaffaldano and Antonio Villaseñor.

References

- Adiyaman, O., Chorowicz, J., Arnaud, O.N., Gündoğdu, M.N., Gourgaud, A., 2001. Late Cenozoic tectonics and volcanism along the North Anatolian Fault: new structural and geochemical data. *Tectonophysics* 338, 135–165.
- Aki, K., Lee, W.H.K., 1976. Determination of three-dimensional velocity anomalies under a seismic array using first P arrival times from local earthquakes—I. A homogeneous initial model. *J. Geophys. Res.* 81, 4381–4399.
- Allam, A.A., Ben-Zion, Y., 2012. Seismic velocity structures in the southern California plate-boundary environment from double-difference tomography. *Geophys. J. Int.* 190, 1181–1196.
- Bakırcı, T., Yoshizawa, K., Özer, M.F., 2012. Three-dimensional S wave structure of the upper mantle beneath Turkey from surface wave tomography. *Geophys. J. Int.* 190, 1058–1076.
- Barka, A.A., 1992. The North Anatolian fault zone. *Ann. Tect.* 164–195, 6.
- Ben-Zion, Y., 2008. Collective behavior of earthquakes and faults: continuum-discrete transitions, progressive evolutionary changes, and different dynamic regimes. *Rev. Geophys.* 46, <http://dx.doi.org/10.1029/2008RG00260>.
- Biryol, C.B., Beck, S., Zandt, G., Ozacar, A.A., 2011. Segmented African lithosphere beneath the Anatolian region inferred from teleseismic P-wave tomography. *Geophys. J. Int.* 184, 1037–1057.
- Bleibinhaus, F., Hole, J.A., Ryberg, T., 2007. Structure of the California Coast Ranges and San Andreas Fault at SAFOD from seismic waveform inversion and reflection imaging. *J. Geophys. Res.* 112, <http://dx.doi.org/10.1029/2006JB004611>.
- Bozdağ, E., Trampert, J., 2008. On crustal corrections in surface wave tomography. *Geophys. J. Int.* 172, 1066–1082.
- Bozkurt, E., 2001. Neotectonics of Turkey—a synthesis. *Geodyn. Acta* 14, 3–30.
- Capdeville, Y., Guillot, L., Marigo, J.J., 2010a. 1-D nonperiodic homogenization for the wave equation. *Geophys. J. Int.* 181, 897–910.
- Capdeville, Y., Guillot, L., Marigo, J.J., 2010b. 2-D nonperiodic homogenization to upscale elastic media for P-SV waves. *Geophys. J. Int.* 182, 903–922.
- Chen, P., 2011. Full-wave seismic data assimilation: theoretical background and recent advances. *Geophys. J. Int.* 168, 1527–1552.
- Chen, P., Zhao, L., Jordan, T.H., 2007. Full 3D tomography for the crustal structure of the Los Angeles region. *Bull. Seismol. Soc. Am.* 97, 1094–1120.
- Currenti, G., Del Negro, C., Ganci, G., Williams, C.A., 2008. Static stress changes induced by the magmatic intrusions during the 2002–2003 Etna eruption. *J. Geophys. Res.* 113, <http://dx.doi.org/10.1029/2007JB005301>.
- Egeran, N., Lahn, E., 1944. Note sur la carte sismique de la Turquie au 1: 2.400.000. *Maden Tekt. Arama Enst. Mecmuası* 2 (32), 279–289.
- Ferreira, A.M.G., Woodhouse, J.H., Visser, K., Trampert, J., 2010. On the robustness of global radially anisotropic surface wave tomography. *J. Geophys. Res.* 115, <http://dx.doi.org/10.1029/2009JB006716>.
- Fichtner, A., Bunge, H.P., Igel, H., 2006. The adjoint method in seismology—I. Theory. *Phys. Earth Planet. Inter.* 157, 86–104.
- Fichtner, A., Kennett, B.L.N., Igel, H., Bunge, H.P., 2008. Theoretical background for continental- and global-scale full-waveform inversion in the time-frequency domain. *Geophys. J. Int.* 175, 665–685.
- Fichtner, A., Kennett, B.L.N., Igel, H., Bunge, H.P., 2009. Full seismic waveform tomography for upper-mantle structure in the Australasian region using adjoint methods. *Geophys. J. Int.* 179, 1703–1725.
- Fichtner, A., Kennett, B.L.N., Igel, H., Bunge, H.P., 2010. Full waveform tomography for radially anisotropic structure: new insights into present and past states of the Australasian upper mantle. *Earth Planet. Sci. Lett.* 290, 270–280.
- Fichtner, A., Trampert, J., 2011a. Hessian kernels of seismic data functionals based upon adjoint techniques. *Geophys. J. Int.* 185, 775–798.
- Fichtner, A., Trampert, J., 2011b. Resolution analysis in full waveform inversion. *Geophys. J. Int.* 187, 1604–1624.
- Fichtner, A., Trampert, J., Cupillard, P., Saygin, E., Taymaz, T., Capdeville, Y., Villaseñor, A. Multi-scale full waveform inversion. *Geophys. J. Int.*, in press, <http://dx.doi.org/10.1093/gji/ggt118>.
- Huang, W.J., Johnson, K.M., 2012. Strain accumulation across strike-slip faults: investigation of the influence of laterally varying lithospheric properties. *J. Geophys. Res.* 117, <http://dx.doi.org/10.1029/2012JB009424>.
- Karabulut, H., Ozalaybey, S., Taymaz, T., Aktar, M., Selvi, O., Kocaoglu, A., 2003. A tomographic image of the shallow crustal structure in the Eastern Marmara. *Geophys. Res. Lett.* 30, <http://dx.doi.org/10.1029/2003GL018074>.
- King, G.C.P., Hubert-Ferrari, A., Meyer, B.S.S.N., Armijo, R., Bowman, D., 2001. Coulomb interactions and the 17 August 1999 Izmit, Turkey, earthquake. *C. R. Acad. Sci. Ser. A* 333, 557–569.
- Komatitsch, D., Tromp, J., 2002. Spectral-element simulations of global seismic wave propagation, Part I: validation. *Geophys. J. Int.* 149, 390–412.
- Komatitsch, D., Vilotte, J.P., 1998. The spectral element method: an effective tool to simulate the seismic response of 2d and 3d geological structures. *Bull. Seismol. Soc. Am.* 88, 368–392.
- Koulakov, I., Bindi, D., Parolai, S., Grosser, H., Milkereit, C., 2010. Distribution of seismic velocities and attenuation in the crust beneath the North Anatolian Fault (Turkey) from local earthquake tomography. *Bull. Seismol. Soc. Am.* 100, 207–224.
- Lévêque, J.J., Rivera, L., Wittlinger, G., 1993. On the use of the checkerboard test to assess the resolution of tomographic inversions. *Geophys. J. Int.* 115, 313–318.
- Lewis, M.A., Ben-Zion, Y., McGuire, J.J., 2007. Imaging the deep structure of the San Andreas Fault south of Hollister with joint analysis of fault zone head and direct P arrivals. *Geophys. J. Int.* 169, 1028–1042.
- Liu, Q., Tromp, J., 2008. Finite-frequency sensitivity kernels for global seismic wave propagation based upon adjoint methods. *Geophys. J. Int.* 174, 265–286.
- Lyakhovskiy, V., Ben-Zion, Y., 2009. Evolving geometrical and material properties of fault zones in a damage rheology model. *Geochem. Geophys. Geosyst.* 10, <http://dx.doi.org/10.1029/2009GC002543>.
- McGuire, J., Ben-Zion, Y., 2005. High-resolution imaging of the Bear Valley section of the San Andreas Fault at seismogenic depth with fault-zone head waves and relocated seismicity. *Geophys. J. Int.* 163, 152–164.
- Meier, U., Curtis, A., Trampert, J., 2007. Fully nonlinear inversion of fundamental mode surface waves for a global crustal model. *Geophys. Res. Lett.* 34, <http://dx.doi.org/10.1029/2007GL030989>.
- Okay, A.I., Tüysüz, O., 1999. Tethyan sutures of northern Turkey. *Geol. Soc. London (Spec. Publ.)* 156, 475–515.
- Öztürk, S., Destur, M., Karlı, M., 2006. Heat Flow Map of Turkey, 1:2,000,000. General Directorate of Mineral Research and Exploration, Department of Geophysical Exploration, Ankara, Turkey.
- Parsons, T., Toda, S., Stein, R.S., Barka, A.A., Dieterich, J.H., 2000. Heightened odds of large earthquakes near Istanbul: an interaction-based probability calculation. *Science* 288, 661–665.
- Rickers, F., Fichtner, A., Trampert, J., The Iceland—Jan Mayen plume system and its impact on mantle dynamics in the North Atlantic region: evidence from full-waveform inversion. *Earth Planet. Sci. Lett.*, in preparation.
- Ritsema, J., vanHeijst, H., Woodhouse, J.H., 1999. Complex shear wave velocity structure imaged beneath Africa and Iceland. *Science* 286, 1925–1928.
- Salaün, G., Pedersen, H.A., Paul, A., Farra, V., Karabulut, H., Hatzfeld, D., Papazachos, C., Childs, D.M., Pequegnat, C., 2012. The SIMBAAD Team, 2012. High-resolution surface wave tomography beneath the Aegean-Anatolia region: constraints on upper-mantle structure. *Geophys. J. Int.* 190, 406–420.
- Saunders, P., Priestley, K., Taymaz, T., 1998. Variations in the crustal structure beneath western Turkey. *Geophys. J. Int.* 134, 373–389.
- Şengör, A.M.C., Tüysüz, C., Sakiç, M., Eyidoğan, H., Görür, N., Le Pichon, X., Rangin, C., 2005. The North Anatolian Fault: a new look. *Ann. Rev. Earth Planet. Sci.* 33, 37–112.
- Siebert, L., Simkin, T., 2002. Volcanoes of the world: an illustrated catalog of Holocene volcanoes and their eruptions. Smithsonian Institution, Global Volcanism Program Digital Information Series, (<http://www.volcano.si.edu/world/>).
- Stein, R.S., Barka, A.A., Dieterich, J.H., 1997. Progressive failure on the North Anatolian Fault since 1939 by earthquake stress triggering. *Geophys. J. Int.* 128, 594–604.
- Takeuchi, C.S., Fialko, Y., 2012. Dynamic models of interseismic deformation and stress transfer from plate motion to continental transform faults. *J. Geophys. Res.* 117, <http://dx.doi.org/10.1029/2011JB009056>.
- Tape, C., Liu, Q., Maggi, A., Tromp, J., 2010. Seismic tomography of the southern California crust based upon spectral-element and adjoint methods. *Geophys. J. Int.* 180, 433–462.
- Tarantola, A., 1988. Theoretical background for the inversion of seismic waveforms, including elasticity and attenuation. *Pure Appl. Geophys.* 128, 365–399.
- Tone, S., Miyatake, T., Hikima, K., Kato, A., 2009. Change of static stress fields from earthquake rupture in heterogeneous crustal structure. *J. Seismol. Soc. Jpn.* 62, 97–107.
- Tromp, J., Tape, C., Liu, Q., 2005. Seismic tomography, adjoint methods, time reversal and banana-doughnut kernels. *Geophys. J. Int.* 160, 195–216.

- van Hinsbergen, D.J.J., Kaymakci, N., Spakman, W., Torsvik, T.H., 2010. Reconciling the geological history of western Turkey with plate circuits and mantle tomography. *Earth Planet. Sci. Lett.* 297, 674–686.
- Vanacore, E., Taymaz, T., Saygin, E., 2013. Moho structure of the Anatolian plate from receiver function analysis. *Geophys. J. Int.* 193, <http://dx.doi.org/10.1093/gji/ggs107>.
- Yolsal-Çevikbilen, S., Biryol, C.B., Beck, S., Zandt, G., Taymaz, T., Adiyaman, H.E., Özacar, H.E., 2012. 3-D crustal structure along the North Anatolian Fault Zone in north-central Anatolia revealed by local earthquake tomography. *Geophys. J. Int.* 188, 819–849.
- Zhao, S., Muller, R.D., Takahashi, Y., Kaneda, Y., 2004. 3-D finite-element modelling of deformation and stress associated with faulting: effect of inhomogeneous crustal structures. *Geophys. J. Int.* 157, 629–644.
- Zhu, H., Bozdağ, E., Peter, D., Tromp, J., 2012. Structure of the European upper mantle revealed by adjoint tomography. *Nat. Geosci.* 5, 493–498.